Int. J. Wildland Fire 2(3): 99-114, 1992

Atmospheric Simulations of Extreme Surface Heating Episodes on Simple Hills

W. E. Heilman

USDA Forest Service, 1407 South Harrison Road, East Lansing, MI 48823
Tel. 517 355-7740; Fax 517 355-5121

Abstract. A two-dimensional nonhydrostatic atmospheric model was used to simulate the circulation patterns (wind and vorticity) and turbulence energy fields associated with lines of extreme surface heating on simple two-dimensional hills. Heating-line locations and ambient crossflow conditions were varied to qualitatively determine the impact of terrain geometry on the development of buoyancy-induced horizontal roll vortices and their turbulence structures. The model simulations indicate that the type of induced circulation that develops near a line of extreme surface heating on a simple hill is very dependent on the location of the heating line. Heating lines located on the crests of simple hills produced symmetric horizontal roll vortices with large values of turbulent kinetic energy. Symmetric vortices did not develop over heating lines located on the slopes of the hills. The introduction of a light ambient crossflow radically changed the circulation and turbulence structures. Simulated vorticity and turbulence energy values over a heating line located on the windward slope were very different than those observed over heating lines located on the crest or leeward slope. A low-level vortex developed just downwind of the windward-slope heating line when a light ambient crossflow was introduced, and this vortex became stronger as the steepness of the hill was increased. Although field data are not available to confirm the model results, the simulations suggest that terrain effects play an important role in the development and destruction of vortices near lines of extreme surface heating, especially when a light ambient crossflow is introduced. These effects have implications for fire-fighter safety in actual wildland fire episodes.

Keywords: Nonhydrostatic atmospheric model; Circulation; Vorticity; Turbulence; Terrain.

Introduction

The effects of varying terrain on low-level atmospheric circulations have been well-documented. Observations in both the stable and unstable atmospheric boundary layer over complex terrain have been extensively reported in the literature (e.g. Manins and Sawford 1979; Banta and Cotton 1981; Horst and Doran 1982, 1986; Gudiksen 1983; Whiteman and Barr 1986; Barr and Orgill 1989; Clements *et al.* 1989; Dobosy *et al.* 1989; Stone and Hoard 1989). In addition to the observational studies, there have been many numerical modeling attempts at simulating mesoscale and boundary-layer flow in regions of complex terrain (e.g. Mahrer and Pielke 1975; Rao and Snodgrass 1981; Yamada 1981, 1983; Bader and McKee 1983; Banta 1984, 1986; McNider and Pielke 1984; Bader and Whiteman 1989; Leone and Lee 1989; Yamada and Bunker 1989; Heilman and Takle 1991). These studies have attempted to provide a better understanding of the natural atmospheric mean and turbulent structures associated with flow over complex terrain.

Of particular concern to those involved in fighting wildland fires in regions of complex terrain is the role of terrain irregularities in affecting the behavior of fire activity. The intense heat release in a burning region generates a local microclimate with induced circulation patterns that can affect the movement of flames, firebrands, and smoke. For example, horizontal roll vortices have been observed and modeled over actual and simulated wildland fires (Schaefer 1957; Church *et al.* 1980; Luti 1980, 1981; Haines 1982; Haines and Smith 1987; Heilman and Fast 1991a, 1991b). Modeling and experimental studies indicate that the ambient wind conditions superimposed on the buoyancy-induced flow can have a major impact on the resulting mean flow and turbulence structure in the vicinity of the surface heating (Smith *et al.* 1986, 1989; Heilman and Fast 1991a, 1991b). Vortex development and its sustentation were found to be very

sensitive to ambient crossflow wind speeds. There are many possible reasons for variations in low-level wind speeds, including terrain irregularities. The presence of terrain irregularities in wildland fire areas can further complicate the low-level circulation patterns that develop in response to the extreme heat release.

Vortex development along the flanks of wildland fires can pose an extreme threat to fire-fighters in the vicinity if flames and firebrands are caught in the circulation. Because terrain irregularities can alter low-level circulations, vortex development and behavior along the flanks of wildland fires in complex terrain may be quite different than what is observed over relatively flat terrain. Understanding these differences should aid in developing safer strategies for fighting wildland fires in complex terrain regions. Church *et al.* (1980) have shown that the development of horizontal roll vortices is controlled by the mechanisms of horizontal vorticity reorientation and stretching, vertical vorticity concentration and amplification, and buoyancy. This study deals specifically with the buoyancy mechanism and provides some simple two-dimensional numerical simulations of atmospheric behavior over lines of extreme surface heating located at various positions on two different types of hills. The role of ambient crossflows in affecting vortex development over the different terrain geometries for different locations of surface heating is investigated. The results are qualitatively analyzed in terms of possible implications for fire-fighter safety.

Model Overview

In order to resolve the boundary-layer circulations that develop in the vicinity of extreme heat release associated with wildland fires, it is necessary to use a numerical model that will allow for grid-spacings on the order of 100 m or less in the horizontal. Furthermore, the model must be able to account for terrain irregularities. The use of a hydrostatic model under these conditions is prohibited because many of the underlying assumptions regarding a hydrostatic atmosphere are violated when simulating phenomena with horizontal scales less than 5 km (Martin and Pielke 1983; Song *et al.* 1985). In addition, hydrostatic models are not adequate for simulating extreme convection episodes in regions of complex terrain. These constraints on hydrostatic models force the use of nonhydrostatic boundary-layer models.

A two-dimensional nonhydrostatic atmospheric model was developed from the three-dimensional hydrostatic model of McCorcle (1988) and Fast and McCorcle (1990). Atmospheric variables predicted in this hydrostatic model include the horizontal velocity components, potential temperature, specific humidity, and turbulent kinetic energy (TKE). The vertical velocity component and the atmospheric pressure are diagnosed from the continuity and hydrostatic equations, respectively. This model was made nonhydrostatic by adding a prognostic equation for the vertical velocity and a Poisson equation for the dynamic pressure perturbations. The governing equations were also transformed to a non-orthogonal terrain-following coordinate system to allow for easy integration of the equations over complex terrain. The complete set and description of the two-dimensional atmospheric governing equations used in this study can be found in Heilman and Fast (1991b).

Computational Processes

Numerical Methods

The governing equations are approximated with both finite-difference and finite-element techniques. Finite differences are used to approximate advection, pressure gradient, TKE shear production, and TKE buoyancy production terms. Vertical diffusion terms are represented by a Galerkin finite-element expression, which controls nonlinear computational instability problems. The prognostic equations are integrated forward in time through the use of the Crank-Nicholson method, while the Poisson equation for dynamic pressure perturbations is solved at each time step by an iterative successive over-relaxation procedure.

Model Domain

Two different terrain features are introduced into the model domain, which spans a 2.0 km wide by 1.8 km high vertical plane. The two terrain features are defined by a cosine-squared shaped two-dimensional hill:

$$h\left[\cos^2\left(\frac{\pi x'}{W}\right)\right] \qquad (1)$$

where h is the height of the hill crest, W is the total width of the hill, and x' is the horizontal distance from the crest of the hill. For the simulations in this study, W is given a value of 800 m, and h is given values of 50 m and 100 m. These terrain geometries result in maximum slope angles of about 11° (hill #1) and 21° (hill #2).

A non-orthogonal terrain-following grid structure is applied to the model domain. A logarithmic vertical grid spacing is used from the surface up to a height of about 100 m, with an equally-spaced grid from there to the model top. Over the crests of the two-dimensional hills, the minimum vertical grid spacings for the 50 m and 100 m high hills are about 0.17 m and 0.16 m, respectively.

The horizontal grid spacing is set at 50 m over the entire domain. A total of 656 grid points are used in the simulations, with 41 grid points in the horizontal direction and 16 grid points in the vertical direction.

The model simulations are carried out for a simulated period of 90 s. The time step is set at 0.05 s in order to preserve numerical stability for the fine grid structure utilized in this study.

Boundary and Initial Conditions

In order to examine the role of a simple two-dimensional hill in affecting the circulation patterns that develop in response to isolated lines (homogeneous in the y-direction) of extreme surface heating, a constant surface potential temperature of 1500° K is introduced at three different locations on hill #1 and hill #2 (on the crest, on the leeward slope, and on the windward slope). Potential temperatures at other locations on the surface are computed at each time step from a soil heat-flux equation. Surface-layer values for other mean variables and the turbulence-related variables are calculated from the relations of Paulson (1970), Businger *et al.* (1971), and Mellor and Yamada (1974). The dynamic perturbation pressures are assumed to have vertical gradients equal to zero at the surface.

The wind field is assumed to be geostrophic at the model top, where geostrophic wind components are externally specified. The vertical velocity component is set to zero at the model top. The potential temperature, TKE, and dynamic pressure perturbations are all assumed to have vertical gradients equal to zero at the top of the modeled domain. Along the lateral boundaries, zero-gradient conditions in the horizontal are used for all modeled variables except the pressure perturbations; they are set to zero at the lateral boundary grid points.

The impact of varying crossflow wind speeds on the induced circulation patterns associated with lines of extreme surface heating is investigated by introducing initial logarithmic x-component wind (U) profiles with friction velocities (u_*) of 0.0 m s^{-1}, 0.05 m s^{-1}, 0.1 m s^{-1}, and 0.2 m s^{-1}. These friction velocities result in model-top U velocities of 0.0 m s^{-1}, 1.43 m s^{-1}, 2.86 m s^{-1}, and 5.73 m s^{-1}, respectively. The friction velocity of the y-component of the initial wind field (V) is set to 0.2 m s^{-1} for all simulations. The initial potential temperature field is set at 298° K except at the surface locations where a 1500° K potential temperature is specified. The Mellor and Yamada (1974) turbulence hierarchy is used to diagnose the initial TKE profiles. A dry atmosphere, as well as soil layer is assumed, with an initial soil temperature of 298° K specified everywhere except at the point of heating.

Numerical Results

Hill #1

Figure 1 shows the simulated two-dimensional velocity fields over hill #1 for three different heating-line locations under varying ambient crossflow conditions (initial u_* values of 0.0 m s^{-1}, and 0.1 m s^{-1}). It is clear that symmetric vortices do not develop over the heating lines located on either side of the hill crest when no ambient crossflow is present (see Figs. 1a and 1e). The presence of a sloped surface acts to distort the circulation patterns over the heating lines so that the horizontal placement of maximum updraft speeds at each height above the surface moves toward the crest with altitude. Near the surface, simulated wind vectors have significant horizontal components over the heating lines. Only at a height of about 100 m do the simulated wind directions become largely vertical over the lines of heating. The updraft regions extend upward to about 1000 m, with significant downdraft speeds occurring from about 600 m down to the surface at horizontal distances of about 100 m from the heating-line locations. When the heating lines are located over the steepest portions of the hill, the induced low-level horizontal flow at horizontal distances greater than 100 m from the heating lines is stronger on the downslope sides of the heating lines.

When an ambient crossflow corresponding to an initial friction velocity of 0.1 m s^{-1} is introduced, the simulated circulation patterns associated with the heating lines at x = 800 m and x = 1200 m are quite different from each other, as shown in Figs. 1b and 1f. The updraft wind speeds are stronger when the heating line is located over the windward slope than when located over the leeward slope. The sloped terrain acts to reinforce upward vertical motion associated with buoyancy effects over the windward slope and to diminish the upward motion over the leeward slope. The more intense updraft speeds associated with the heating line on the windward slope also generate a stronger low-level recirculation zone downwind of the heating line than with the leeward-slope heating line. For both cases, a low-level wake is generated downwind of the heating lines where induced flow toward the heating lines is diminished due to the ambient crossflow. However, the vertical extent of this wake is larger when the heating line is situated over the windward slope.

Figures 1c and 1d show the effect of an ambient crossflow on the simulated circulation patterns that result when a line of heating is placed at the crest of the hill. For the no-ambient-crossflow case (Fig. 1c), symmetric vortices develop adjacent to the updraft region. These simulated vortices look very similar to the simulated vortices of Heilman and Fast (1991a, 1991b) over flat

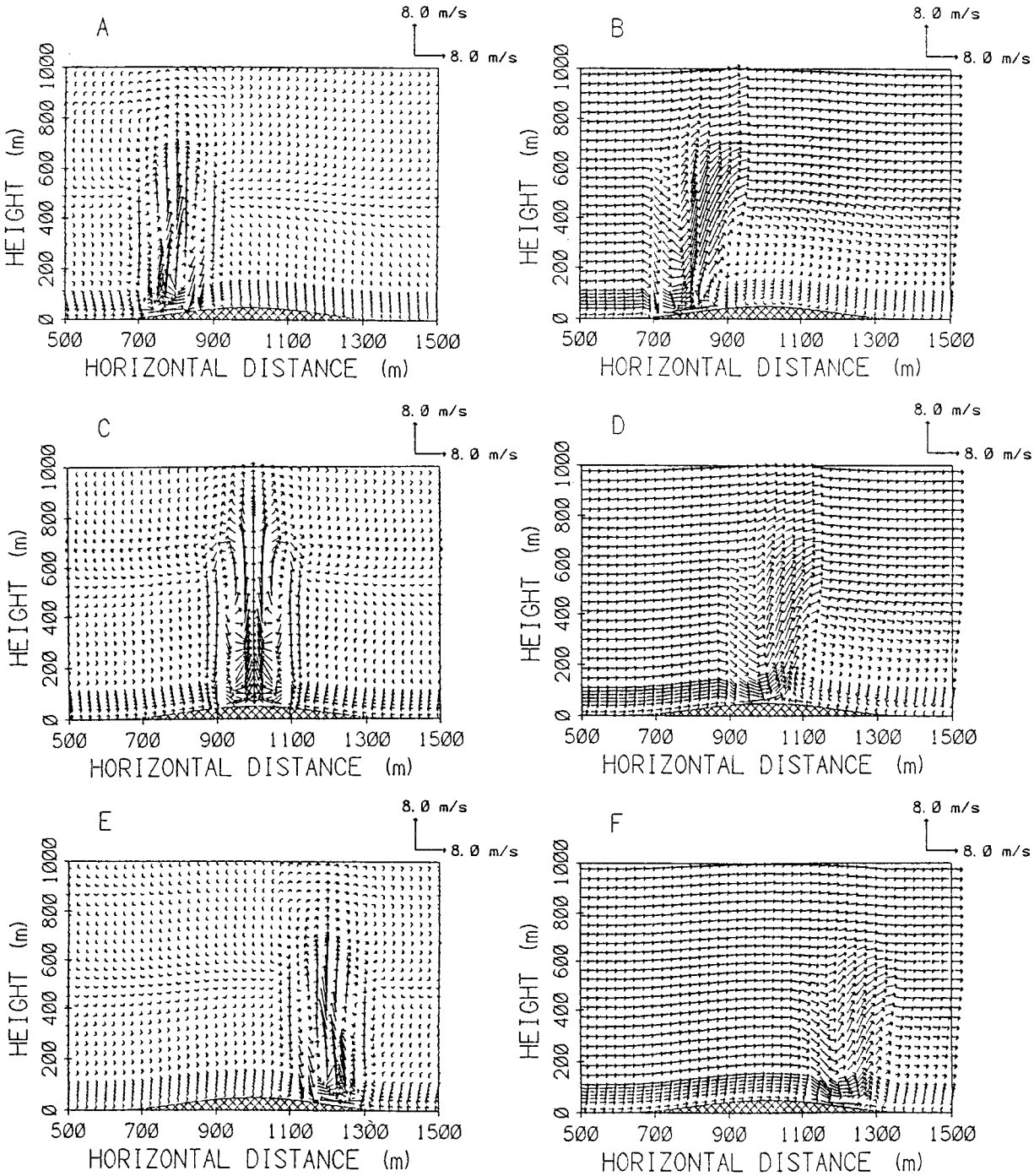

Figure 1. Simulated two-dimensional wind fields over hill #1 after 90 s of simulated time for three different heating-line locations and two different ambient crossflow conditions: (a) windward slope, u_*=0.0 m s^{-1}; (b) windward slope, u_*=0.1 m s^{-1}; (c) crest, u_*=0.0 m s^{-1}; (d) crest, u_*=0.1 m s^{-1}; (e) leeward slope, u_*=0.0 m s^{-1}; (f) leeward slope, u_*=0.1 m s^{-1}.

terrain. Low-level inflow is identical on both sides of the crest, in contrast to the cases where the heating line is situated over the hill slopes. The updraft region over the heating line extends upward to about 1100 m, with significant downdraft speeds occurring at x = 900 m and x = 1100 m from a height of about 600 m down to the surface. When a light ambient crossflow is introduced (initial $u_* = 0.1$ m s^{-1}), the upper-level vortices are destroyed while a low-level vortex immediately downwind of the heating line at the crest remains (Fig. 1d). The wave that develops in the circulation over the heating line is also very similar to the flat-terrain simulations of Heilman and Fast (1991a, 1991b).

A useful method for identifying regions of significant wind shear and curvature in the two-dimensional airflow is an analysis of the two-dimensional relative vorticity field ζ, defined as

$$\zeta = \frac{\partial W}{\partial x} - \frac{\partial U}{\partial z} \quad . \qquad (2)$$

Figures 2a - 2f show the vorticity fields for the corresponding velocity fields of Figs. 1a -1f. The presence of a heating line at the crest of the hill with no ambient crossflow (see Fig. 1c) results in a vorticity field that is characterized by much larger maxima than for heating lines located on the slopes of the hill. In particular, the positive and negative vorticity below an elevation of 100 m to the left and right of the heating line at the crest is very pronounced, due to the tremendous vertical shear in the horizontal wind component. At an elevation of 500 m, positive and negative vorticity maxima appear at x = 975 m and x = 1025 m, respectively, corresponding to the symmetric vortices in Fig. 1c. For heating lines placed on the slopes of the hill (x = 800 m and x = 1200 m) with no ambient crossflow, the vorticity patterns are not symmetric about the heating lines (Figs. 2a and 2e). Instead, a positive (negative) vorticity maximum appears at a height about 75 m above the surface at x = 825 m (x = 1175 m) when the heating line is situated at x = 800 m (x = 1200 m). The upper-level vorticity magnitudes for these cases are much less than for the heating line situated at the crest.

When an ambient crossflow is introduced, the vorticity patterns for the three different heating-line positions exhibit an interesting behavior (Figs. 2b, 2d, and 2f). The crossflow has much more of a dissipative impact on the vorticity when the heating lines are located on the crest and leeward slope. Over the windward slope, vorticity remains significant, especially at x = 850 m and z = 75 m where a low-level recirculation zone exists. With the heating line over the leeward slope, no recirculation zone exists and the overall vorticity is much less. The ambient crossflow also significantly reduces the overall vorticity in the circulation associated with a heating line located at the crest compared to the no-ambient-crossflow case, although the low-level negative vorticity maximum remains at x = 1050 m.

A summary of the vorticity characteristics for all the ambient crossflow simulations on hill #1 is shown in Table 1. The significant reduction in the magnitudes of the positive and negative vorticity maxima is clearly evident for the crest and leeward fireline simulations as the speed of the ambient crossflow increases. However, the magnitudes of the vorticity maxima generally increase or remain fairly constant over the windward slope as the initial friction velocity increases from 0.0 m s^{-1} to 0.1 m s^{-1}. It isn't until u_* is increased to 0.2 m s^{-1} that the vorticity values over the windward slope decrease to relatively small numbers. The locations of the positive and negative vorticity maxima are also affected by increasing ambient crossflow speeds. When the heating line is located on the windward slope or the crest, positive vorticity maxima tend to move to lower elevations as the ambient crossflow speed increases. The opposite appears to happen when the heating line is located over the leeward slope. The picture is somewhat more ambiguous for the negative vorticity maxima. When values of the negative vorticity maxima are less than -0.10 s^{-1}, the elevations of the maxima over the windward slope and crest tend to remain fairly constant as the ambient crossflow increases. Over the leeward slope, the negative vorticity maximum tends to decrease in elevation.

Terrain geometry and ambient crossflow conditions also affect the turbulence energy associated with heating lines located on the surface. Figure 3 shows the simulated turbulent kinetic energy (TKE) fields corresponding to the circulation and vorticity fields depicted in Figs. 1 and 2. The most obvious difference in the TKE fields is the strength of the turbulence over the heating line at the crest of the hill in comparison to the other heating line placements when there is no ambient crossflow (Figs. 3a, 3c, and 3e). The simulated TKE field over the crest also shows two maxima, one about 150 m above the surface, and the other about 475 m above the surface. The large turbulence energy values at upper levels for this case can be attributed to the symmetric nature of the induced circulation where strong upslope flow from both sides of the heating line results in large updraft speeds over the heating line with little low-level horizontal ventilation of heat. More heat is advected upward by the vertical wind component, which in turn causes the upper-level instability and buoyancy to increase. An analysis of the TKE budget terms reveals that buoyancy production dominates and closely resembles the TKE field. Thus, the turbulence associated with extreme surface heating at the crest is closely tied to the stability of the atmosphere

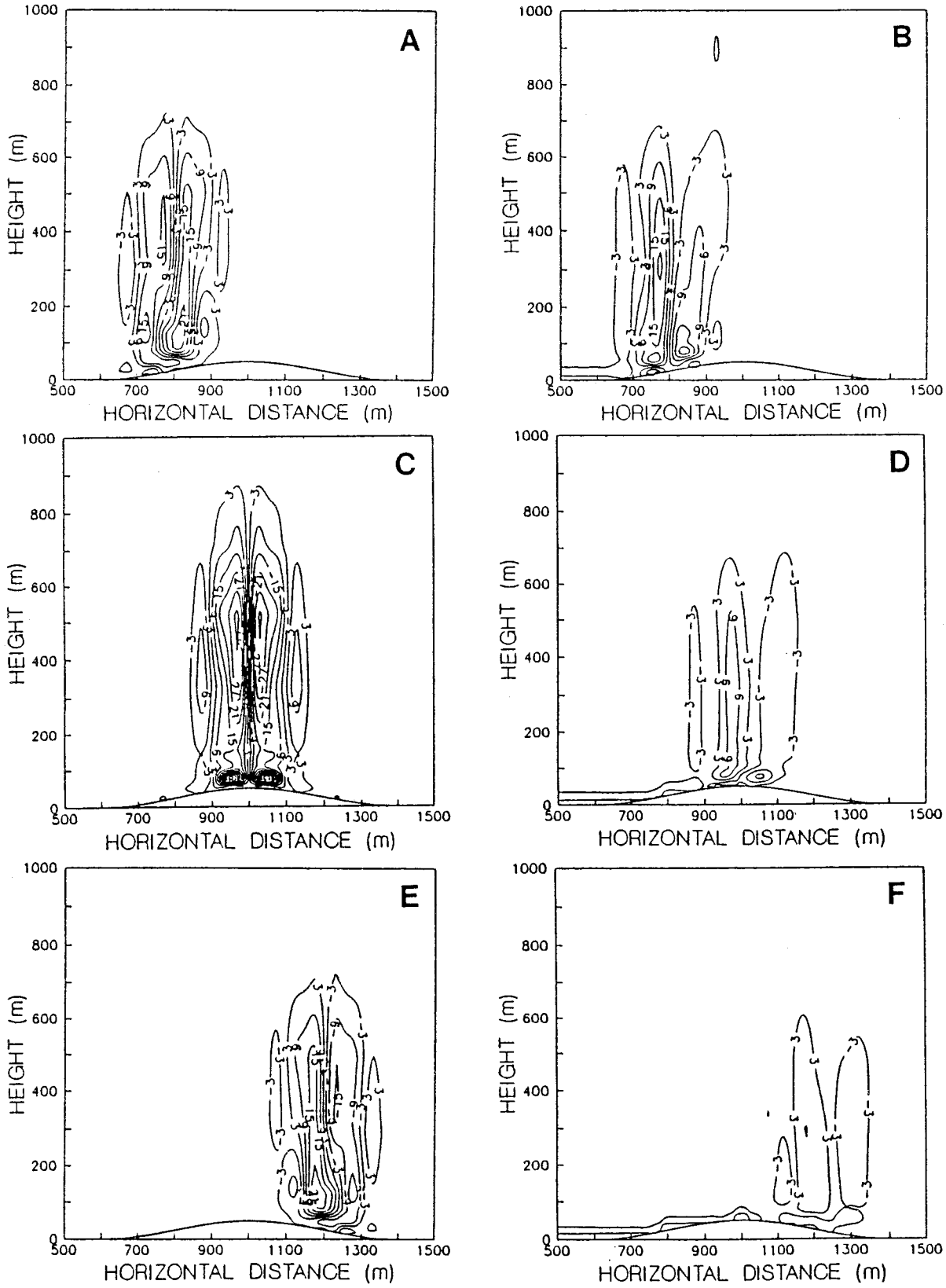

Figure 2. Contour plots of the simulated two-dimensional vorticity (x 100) over hill #1 after 90 s of simulated time for three different heating-line locations and two different ambient crossflow conditions: (a) windward slope, u_a=0.0 m s^{-1}; (b) windward slope, u_a=0.1 m s^{-1}; (c) crest, u_a=0.0 m s^{-1}; (d) crest, u_a=0.1 m s^{-1}; (e) leeward slope, u_a=0.0 m s^{-1}; (f) leeward slope, u_a=0.1 m s^{-1}.

Table 1. Characteristics of the vorticity and TKE over hill #1 after a simulated time of 90 s for the three different heating line locations. The letters A, B, C, and D refer to the initial ambient crossflow friction velocities of 0.0 m s^{-1}, 0.05 m s^{-1}, 0.1 m s^{-1}, and 0.2 m s^{-1}, respectively.

	Heating Line on Windward Slope (x = 800 m)			
	A	B	C	D
Pos. Vort. Max.	0.16 s^{-1}	0.22 s^{-1}	0.21 s^{-1}	0.05 s^{-1}
Location of Pos. Vort. Max.	(725,125) (775,400)	(775,400)	(775,300)	NA
Neg. Vort. Max.	-0.24 s^{-1}	-0.24 s^{-1}	-0.22 s^{-1}	-0.04 s^{-1}
Location of Neg. Vort. Max.	(825,100)	(825,125)	(835,80)	NA
TKE Max.	22 m^2s^{-2}	27 m^2s^{-2}	32 m^2s^{-2}	16 m^2s^{-2}
Vertical Extent of Significant TKE	25 < z < 630	25 < z < 650	25 < z < 500	25 < z < 300
	Heating Line on Crest (x = 1000 m)			
	A	B	C	D
Pos. Vort. Max.	0.33, 0.51 s^{-1}	0.22 s^{-1}	0.11 s^{-1}	0.10 s^{-1}
Location of Pos. Vort. Max.	(975,500) (950,75)	(975,400)	(980,325)	(1075,450)
Neg. Vort. Max.	-0.33, -0.51 s^{-1}	-0.33 s^{-1}	-0.15 s^{-1}	-0.10 s^{-1}
Location of Neg. Vort. Max.	(1025,500) (1050,75)	(1050,75)	(1050,75)	(1125,400)
TKE Max.	55 m^2s^{-2}	32 m^2s^{-2}	26 m^2s^{-2}	16 m^2s^{-2}
Vertical Extent of Significant TKE	50 < z < 700	50 < z < 650	50 < z < 475	50 < z < 325
	Heating Line on Leeward Slope (x = 1200 m)			
	A	B	C	D
Pos. Vort. Max.	0.24 s^{-1}	0.17 s^{-1}	0.09 s^{-1}	0.04 s^{-1}
Location of Pos. Vort. Max.	(1175,100)	(1180,125)	(1180,300)	(1275,300)
Neg. Vort. Max.	-0.16 s^{-1}	-0.15 s^{-1}	-0.06 s^{-1}	-0.04 s^{-1}
Location of Neg. Vort. Max.	(1225,400) (1275,125)	(1260,50)	(1300,300)	(1325,300)
TKE Max.	22 m^2s^{-2}	22 m^2s^{-2}	21 m^2s^{-2}	16 m^2s^{-2}
Vertical Extent of Significant TKE	25 < z < 630	25 < z < 525	25 < z < 400	25 < z < 250

over the heating line, which of course is impacted by the type of circulation that has been induced over the underlying topography.

The simulated TKE fields associated with the heating lines situated on the slopes of the hill (Figs. 3a and 3e) are also controlled to a large extent by the buoyancy production fields. However, these fields do not reflect upper level maxima. Only maxima very near the surface appear in the simulations, with much less turbulence energy characterizing the upper levels. The reduced upper-level TKE values are the result of weaker vertical advection and less instability of the air above the heating lines.

When a light ambient crossflow is introduced (initial $u_* = 0.1$ m s^{-1}), the vertical extent of significant TKE is greatly reduced as updrafts over the heating lines become more horizontal (see Figs. 3b, 3d, and 3f). However, when the heating line is placed on the windward slope, low-level turbulence actually increases. This does not happen with the heating line on the crest or leeward slope. The increased low-level turbulence on the windward slope reflects the impact of mechanical generation of turbulence. As stated previously, the vorticity field over the windward slope in this case remains substantial (see Fig. 2b), indicating that shear effects are still impor-

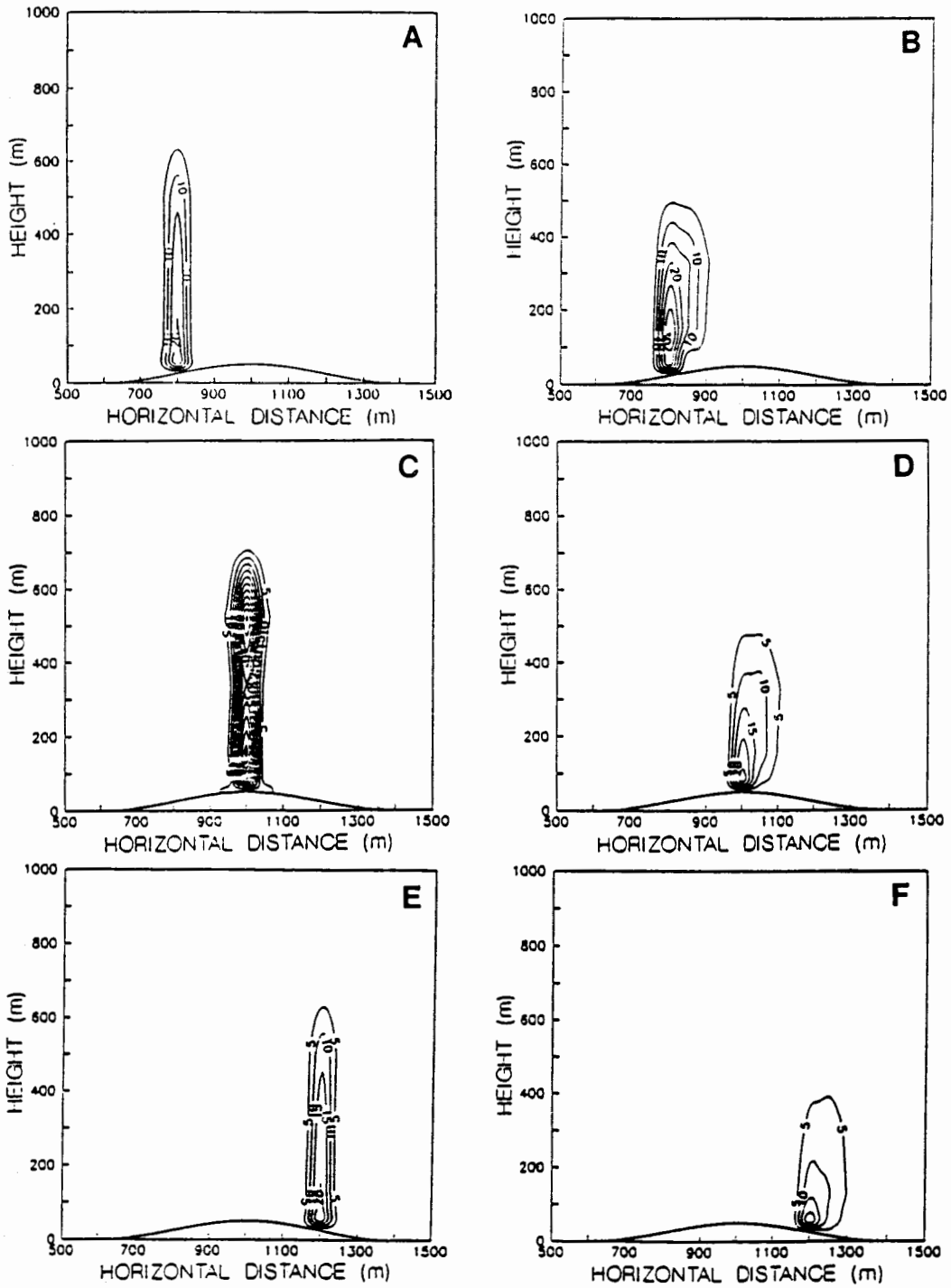

Figure 3. Contour plots of the simulated TKE over hill #1 after 90 s of simulated time for three different heating-line locations and two different ambient crossflow conditions: (a) windward slope, u_*=0.0 m s^{-1}; (b) windward slope, u_*=0.1 m s^{-1}; (c) crest, u_*=0.0 m s^{-1}; (d) crest, u_*=0.1 m s^{-1}; (e) leeward slope, u_*=0.0 m s^{-1}; (f) leeward slope, u_*=0.1 m s^{-1}.

tant. One can also observe the role of horizontal advection near the surface at 850 m < x < 900 m, where less turbulent air is transported into the heating region. The turbulence energy in this region is diminished, while at upper levels at the same horizontal location, the turbulence is enhanced as energy is transported away from the column above the heating line. Over the heating lines on the crest and leeward slopes, upper-level turbulence is substantially reduced when a light ambient crossflow is introduced, especially over the heating line on the crest. The TKE is transported downwind by the ambient crossflow, which also tends to diminish the instability over the heating lines. The terrain geometry at the crest and leeward slope produces simulated low-level circulations induced by extreme surface heating that mechanically produce turbulence to a lesser degree than for a heating line located over the windward slope.

Table 1 summarizes the TKE behavior for simulations of atmospheric conditions over hill #1 for the different ambient crossflow speeds and heating-line placements. Increasing the initial ambient crossflow speed tends to reduce the TKE maxima when the heating line is placed over the crest and leeward slope. However, the TKE maxima increase in magnitude over the windward slope as the initial friction velocity is increased from 0.0 m s^{-1} to 0.1 m s^{-1}. Only when the initial friction velocity is increased to 0.2 m s^{-1} does the TKE maximum over the windward slope decrease in magnitude. For all cases except one, the vertical extent of significant TKE (defined as $e \geq 5$ m^2 s^{-2}) decreases as the ambient crossflow speed increases.

Hill #2

Numerical simulations of the circulation patterns and turbulence structure were also performed for heating lines placed on the surface of a steeper 100 m-high two-dimensional hill. These simulations were carried out to investigate how the steepness of a hill affects the responses of circulation and turbulence fields to different ambient crossflow conditions. Figure 4 shows the two-dimensional wind field for the same ambient crossflow conditions of Figs. 1-3. In general, the steeper hill results in more vigorous circulations, especially at lower levels where terrain effects are most important. The distortion of the flow over the heating lines located at x = 800 m and x = 1200 m (Figs. 4a and 4e) is more pronounced than for the corresponding simulations over hill #1. Stronger upslope and downslope flows characterize the hill #2 simulations. With steeper slopes, the heating line at the crest induces very strong upslope inflow and much stronger updrafts and downdrafts than with hill #1 (Fig. 4c). The upper-level symmetric vortices over the heating line at the crest are also more vigorous with the steeper hill. Finally, the induced inflow toward the heating lines on the downslope sides of the heating lines (x < 700 m and x > 1300 m) is much stronger than the inflow on the upslope sides (x > 900 m and x < 1100 m) when the heating lines are placed on the steepest portions of the hill (x = 800 m and x = 1200 m).

The impact of a non-uniform surface elevation on the circulation patterns resulting from lines of extreme surface heating is clearly evident when comparing the crossflow-wind scenarios for hill #2 (Figs. 4b, 4d, and 4f) and hill #1 (Figs. 1b, 1d, and 1f). The steeper hill slopes enhance the updraft speeds over and downwind of the heating line on the windward side of the crest and diminish the updraft speeds over and downwind of the heating line on the leeward side. With the surface heating line on the windward slope, the low-level recirculation zone at 800 m ≤ x ≤ 900 m is much stronger over hill #2. The circulation patterns resulting from a heating line at the crest of hill #1 and hill #2 in the presence of a light ambient crossflow are very similar, although the upslope flow downwind of the crest is slightly greater over the steeper slope of hill #2.

The simulated vorticity fields over hill #2 are shown in Fig. 5, and support the observation that the steeper hill generally produces more vigorous low-level circulations. A comparison of the positive and negative vorticity maxima for the circulations induced by heating lines on the steepest portions of hill #1 and hill #2 indicates a 37%-50% increase in vorticity magnitudes from hill #1 to hill #2 when no ambient crossflow is present. The increase in vorticity maxima magnitudes is about 10% for heating lines on the crests of the hills with no ambient crossflow. The imposition of a light ambient crossflow (initial $u_* = 0.1$ m s^{-1}) has the most enhancing effect on the circulation associated with the heating line on the windward slope. The positive and negative vorticity maxima magnitudes at these locations increase between 14% and 27% from hill #1 to hill #2. Furthermore, significant vorticity exists at higher altitudes over hill #2 than over hill #1, especially when the heating line is placed on the windward slope. Increasing the steepness of the hill does, however, reduce the low-level negative vorticity at 1000 m < x < 1100 m when the heating line is placed at the crest and a light ambient crossflow is present. The curvature induced in the low-level airflow downwind of the heating line in the presence of a light ambient crossflow is most pronounced when the low-level inflow moves over flatter terrain. As with hill #1, the presence of a light ambient crossflow has a dissipative effect on the vorticity when the heating lines are located on the crest and leeward slopes.

Table 2 summarizes the vorticity maxima behavior for all the ambient crossflow simulations over hill #2. The positive and negative vorticity maxima magnitudes

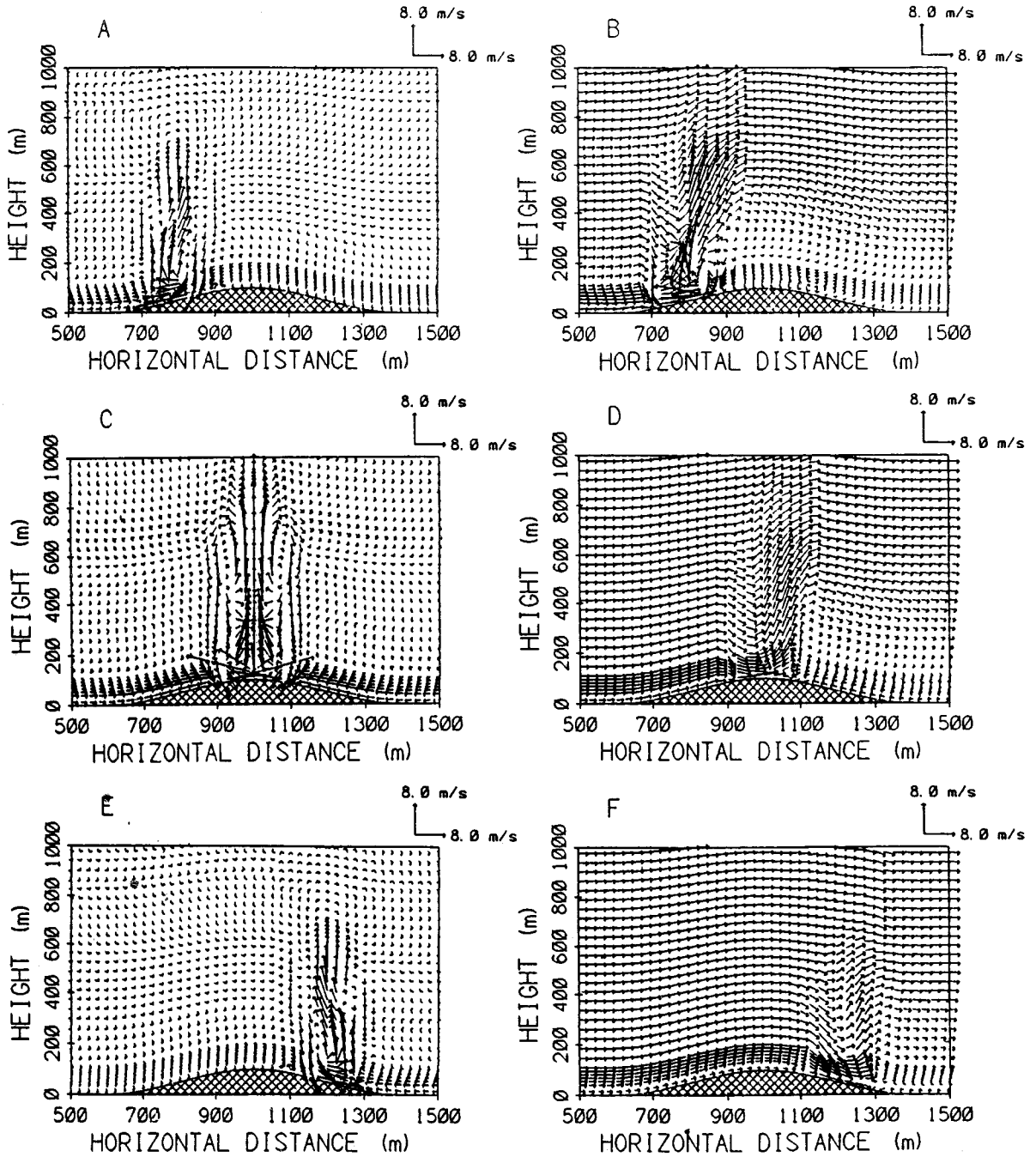

Figure 4. Same as Figure 1 except over hill #2.

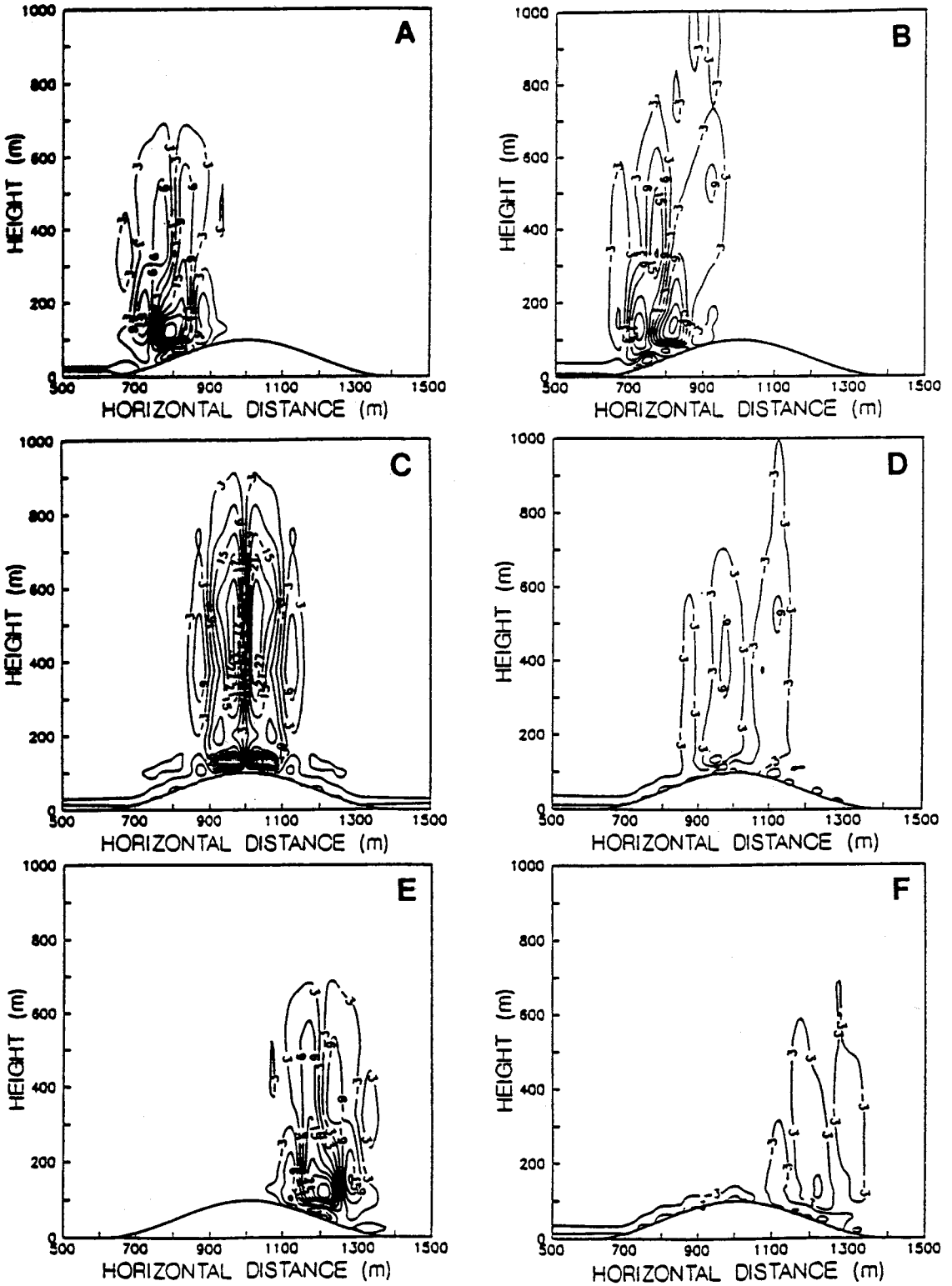

Figure 5. Same as Figure 2 except over hill #2.

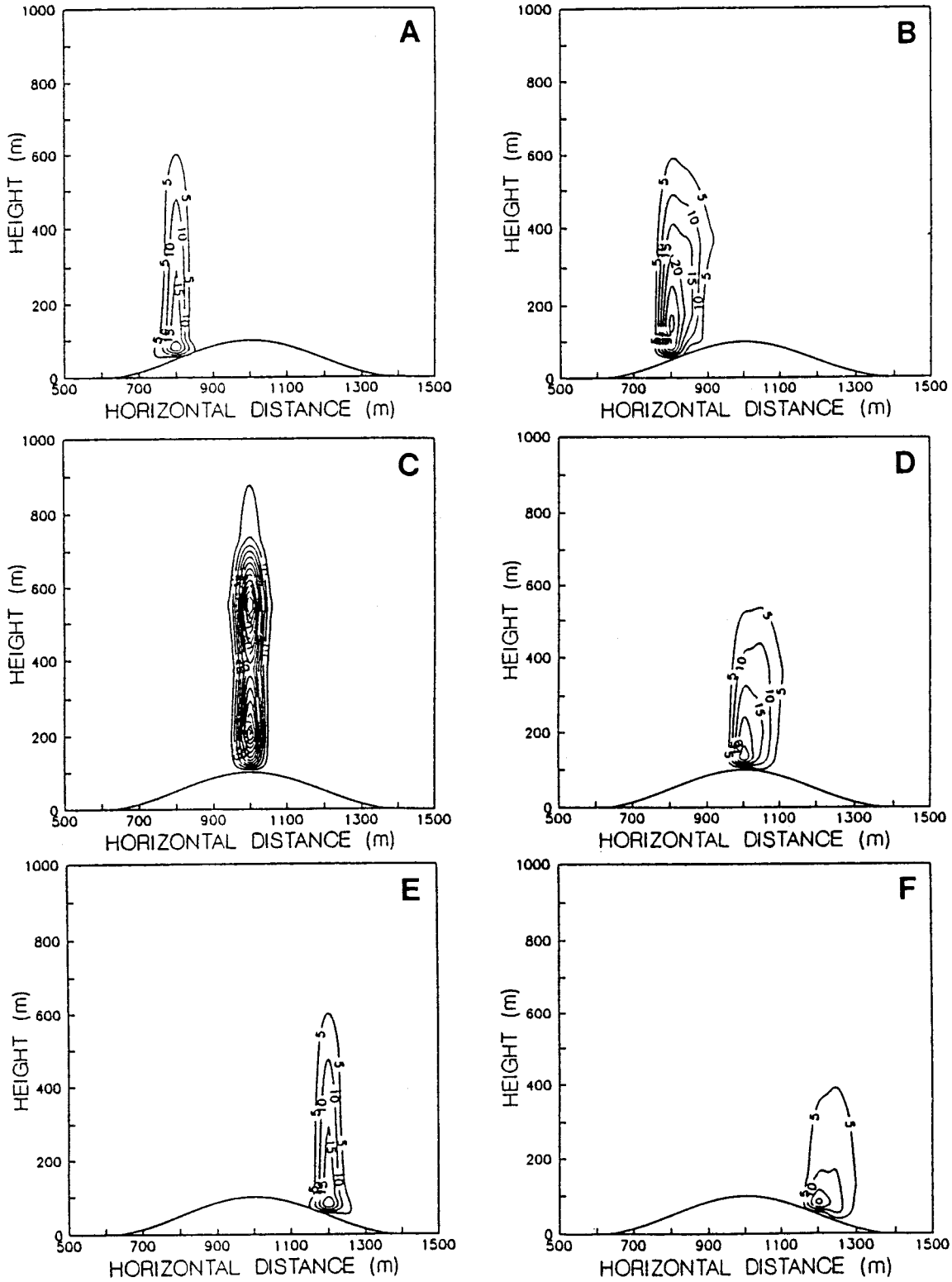

Figure 6. Same as Figure 3 except over hill #2.

show a definite reduction in vorticity for heating lines placed on the crest and leeward slopes when the ambient crossflow speed is increased. Over the windward-slope heating line, all the vorticity maxima magnitudes except one also decrease as the ambient crossflow speed increases. However, the percentage decrease in magnitudes is much less than that for the crest and leeward slope cases when the crossflow wind speed is increased from 0.0 m s^{-1} to 0.1 m s^{-1}. For both hill #1 and hill #2, increasing the initial ambient crossflow friction velocity from 0.1 m s^{-1} to 0.2 m s^{-1} results in a further reduction of overall vorticity.

The movement of the positive and negative vorticity maxima in response to different ambient crossflow conditions is similar to the simulated behavior over hill #1. The positive vorticity maxima tend to move to lower elevations when the heating line is located on the windward slope or crest, and to higher elevations for the leeward-slope, heating-line simulations. The negative vorticity maxima elevations remain fairly constant for the windward slope and crest heating lines as the crossflow speed increases, while the negative maxima tend to move higher over the leeward-slope heating line.

Figure 6 shows the simulated TKE fields over hill #2 for the circulation patterns shown in Fig. 4. As with hill #1, TKE is most significant when the heating line is located on the crest with no ambient crossflow. A double maximum in TKE appears over the heating line on the crest of hill #2, but the upper-level maximum is about 10% larger over hill #2 in comparison to the maximum over the crest of hill #1. With the heating lines on the slopes of the hill and no ambient crossflow, the TKE maxima closely resemble the corresponding TKE maxima over hill #1 (see Tables 1 and 2). However, the enhanced distortion of the low-level circulations over hill #2 results in less upward transport of turbulence and smaller TKE values at upper levels than for hill #1, even though the low-level circulations are more vigorous over hill #2.

The increased steepness of hill #2 in comparison to hill #1 has the most pronounced impact on the TKE values over the windward slope when a light ambient crossflow is present. Instead of a reduction in the vertical extent of significant TKE like that which occurs over the crests and leeward slopes of hill #1 and #2 and over the windward slope of hill #1, the TKE values remain significant over the windward slope of hill #2 at an elevation of 600 m. This can be attributed to the increased orographic "lifting" of the ambient crossflow air over hill #2, which acts to increase the vertical transport of low-level turbulence, increase upper-level instability, and offset the horizontal "ventilation" of upper-level turbulence. In addition, the enhanced low-level recirculation just downwind of the heating line on the surface of the windward slope of hill #2 brings in larger TKE values and offsets the reduction in turbulence resulting from the induced inflow of less turbulent air.

The behavior of the TKE maxima and the vertical extent of significant TKE over hill #2 for the different ambient crossflow conditions are listed in Table 2. When comparing the TKE maxima values over the windward slope of hill #1 and hill #2, it is observed that increasing the hill steepness causes the TKE maximum to remain relatively large even when the initial ambient crossflow friction velocity is increased to 0.2 m s^{-1} (see Table 1).

Summary and Conclusions

A two-dimensional nonhydrostatic model was used to simulate the circulation patterns and turbulence energy fields associated with surface heating lines on two different hills. Ambient crossflow wind speeds were varied to assess the impact of crossflows over irregular terrain on the development of vortices associated with the surface heating lines through the buoyancy mechanism, as outlined by Church *et al.* (1980). Although field data are not available to verify many of the specific results from the numerical simulations, a qualitative assessment of the numerical results should lead to a better understanding of the atmospheric dynamics near firelines on simple hills.

The results from the present simulations suggest that symmetric horizontal roll vortices that have been simulated and observed over flat terrain under calm crossflow conditions (Haines 1982; Heilman and Fast 1991a, 1991b) are less likely to develop on the slopes of simple hills. The presence of a sloped surface alters the induced low-level inflow adjacent to the heating lines so that the inflow is no longer symmetric about the heating lines. This results in maximum updrafts that appear at different horizontal locations as one moves upward in elevation over the heating lines. The simulations indicated that horizontal roll vortices still develop, but they are no longer symmetric and are less vigorous.

Heating lines that exist on the crests of simple hills appear to generate buoyancy-induced horizontal roll vortices that become stronger when found on hills with steeper slopes. The simulations indicate that hills with steeper slopes produce enhanced upslope flows and more vigorous induced circulations above the surface heating lines. The enhanced low-level inflow increases the updraft speeds and vertical extent of upward motion. The increased updraft speeds, in turn, generate stronger compensatory downdrafts at horizontal distances of about 100 m from the heating lines.

The presence of a light ambient crossflow has a considerable impact on the vorticity of the atmosphere in the vicinity of the surface heating lines. The simulations

indicate that the location of extreme surface heating on a simple hill will influence the vortex activity in the boundary layer surrounding the region of heating when an ambient crossflow is present. Furthermore, the size of the hill plays a major role in affecting the vorticity over a line of heating, especially when the heating line is located on the windward slope of the hill. Upper-level vortices are generally destroyed by the light ambient crossflows, but low-level vortices downwind of heating lines on the windward slopes of hill can persist and be quite intense. The intensity of these low-level recirculations is influenced by the underlying terrain geometry, with the more intense vortices existing over steeper slopes. Vortex activity associated with heating lines on the crests and leeward slopes of hills is substantially diminished when an ambient crossflow is present, especially over steeper hills.

The results from these simulations of vortex development and the influence of ambient crossflows on vortex behavior are compatible with previous wind-tunnel observations of horizontal roll vortices (Haines and Smith 1992). The experiments indicate that changes in the

Table 2. Characteristics of the vorticity and TKE over hill #2 after a simulated time of 90 s for the three different heating line locations. The letters A, B, C, and D refer to the initial ambient crossflow friction velocities of 0.0 m s^{-1}, 0.05 m s^{-1}, 0.1 m s^{-1}, and 0.2 m s^{-1}, respectively.

	Heating Line on Windward Slope (x = 800 m)			
	A	B	C	D
Pos. Vort. Max.	0.22 s^{-1}	0.27 s^{-1}	0.24 s^{-1}	0.17 s^{-1}
Location of Pos. Vort. Max.	(725,150)	(725,140)	(725,125)	(760,75)
Neg. Vort. Max.	-0.36 s^{-1}	-0.34 s^{-1}	-0.28 s^{-1}	-0.09 s^{-1}
Location of Neg. Vort. Max.	(790,125)	(800,110)	(825,140)	(840,100)
TKE Max.	22 m^2s^{-2}	27 m^2s^{-2}	31 m^2s^{-2}	27 m^2s^{-2}
Vertical Extent of Significant TKE	50 < z < 600	50 < z < 625	50 < z < 600	50 < z < 350
	Heating Line on Crest (x = 1000 m)			
	A	B	C	D
Pos. Vort. Max.	0.33, 0.56 s^{-1}	0.22 s^{-1}	0.11 s^{-1}	0.10 s^{-1}
Location of Pos. Vort. Max.	(975,500) (950,125)	(975,425)	(980,400)	(1075,550)
Neg. Vort. Max.	-0.32, -0.57 s^{-1}	-0.17 s^{-1}	-0.12 s^{-1}	-0.11 s^{-1}
Location of Neg. Vort. Max.	(1025,500) (1050,125)	(1075,500)	(1140,525)	(1150,500)
TKE Max.	60 m^2s^{-2}	31 m^2s^{-2}	27 m^2s^{-2}	20 m^2s^{-2}
Vertical Extent of Significant TKE	100 < z < 880	100 < z < 690	100 < z < 550	100 < z < 425
	Heating Line on Leeward Slope (x = 1200 m)			
	A	B	C	D
Pos. Vort. Max.	0.36 s^{-1}	0.23 s^{-1}	0.10 s^{-1}	0.05 s^{-1}
Location of Pos. Vort. Max.	(1210,125)	(1215,125)	(1225,130)	(1225,800)
Neg. Vort. Max.	-0.22 s^{-1}	-0.11 s^{-1}	-0.06 s^{-1}	-0.06 s^{-1}
Location of Neg. Vort. Max.	(1275,150)	(1280,275)	(1300,325)	(1325,300)
TKE Max.	22 m^2s^{-2}	21 m^2s^{-2}	21 m^2s^{-2}	18 m^2s^{-2}
Vertical Extent of Significant TKE	50 < z < 600	50 < z < 500	50 < z < 400	50 < z < 250

mean wind direction can produce crossflow components that radically change the vorticity structure in the vicinity of heating lines on flat surfaces. In particular, the experiments indicate that crossflow winds create low-level vorticity maxima downwind of lines of extreme surface heating like those which occur in wildland fires. These low-level vorticity maxima could pose a potential threat to fire-fighter safety if flames and firebrands are caught in the circulations. It is on windward facing slopes where simulations indicate a significant potential for enhanced low-level vortices.

Terrain irregularities and ambient crossflow conditions also affect the atmospheric turbulence structure near lines of extreme surface heating. Under calm ambient crossflow conditions, steeper hills tend to increase the vertical extent of significant turbulence over heating lines located on the crests of the hills. The stronger upslope flow generated over the slopes of steeper hills increases the updraft speeds associated with the heating line at the crest. Stronger updraft speeds lead to an increase in upward vertical advection of turbulence and heat, which also increases upper-level instability and buoyancy generation of turbulence.

In contrast to the turbulence conditions over heating lines on the crests of steeper hills during calm ambient crossflow conditions, steeper hills result in *smaller* upper-level turbulence values over heating lines located on the slopes of the hills under the same calm crossflow conditions. The increased distortion of the low-level flow over steeper hills reduces updraft speeds over the heating lines on the slopes, thereby reducing the vertical extent of significant turbulence and upper-level generation of turbulence by buoyancy effects.

The presence of an ambient crossflow tends to reduce the magnitude and vertical extent of turbulence energy over heating lines located on the crests and leeward slopes of hills. However, over the windward slopes, a light ambient crossflow causes turbulence energy to actually *increase* just above the heating lines. Furthermore, simulations indicate that steeper hills tend to keep upper-level turbulence significant over heating lines located on windward slopes when an ambient crossflow is present.

The results from this numerical study indicate some important qualitative differences in the atmospheric mean and turbulence structures associated with the location of surface heating lines on different types of simple hills under different ambient crossflow conditions. The two-dimensional model results should not be viewed as forecasts of circulations in the vicinity of real firelines. Actual conditions near firelines in regions of complex terrain will be much more complicated and chaotic than what is simulated by the two-dimensional model used in this study. Furthermore, vortices that develop in actual wildland fire episodes are also influenced by horizontal vorticity reorientation and stretching and vertical vorticity concentration and amplification. The present simulations only address the buoyancy mechanism. Nevertheless, they reveal the importance of even simple terrain configurations in affecting buoyancy-induced circulations near lines of extreme surface heating. Terrain irregularities are observed to be particularly important when crossflow winds are present. Before definitive statements can be made regarding the behavior of the atmosphere near real firelines in regions of complex terrain under varying crossflow conditions and the necessary precautions for those involved in controlling wildland fires, three-dimensional model simulations must be performed and compared with field observations. However, the simulations do suggest that terrain geometry should not be ignored when predicting the development of horizontal roll vortices and their associated turbulence structures.

References

Bader, D. C., and C. D. Whiteman. 1989. Numerical simulation of cross-valley plume dispersion during the morning transition period. Journal of Applied Meteorology 28:652-664.

Bader, D. C., and T. B. McKee. 1983. Dynamical model simulation of the morning boundary layer development in deep mountain valleys. Journal of Climate and Applied Meteorology 22:341-351.

Banta, R. M. 1984. Daytime boundary layer evolution over mountainous terrain. Part 1: Observations of the dry circulations. Monthly Weather Review 112:509-522.

Banta, R. M. 1986. Daytime boundary layer evolution over mountainous terrain. Part 2: Numerical studies of upslope flow duration. Monthly Weather Review 114:1112-1130.

Banta, R. M., and W. R. Cotton. 1981. An analysis of the structure of local wind systems in a broad mountain basin. Journal of Applied Meteorology 20:1255-1266.

Barr, S., and M. M. Orgill. 1989. Influence of external meteorology on nocturnal valley drainage winds. Journal of Applied Meteorology 28:497-517.

Businger, J. A., J. C. Wyngaard, Y. Izumi, and E. F. Bradley. 1971. Flux-profile relationships in the atmospheric surface layer. Journal of the Atmospheric Sciences 28:181-189.

Church, C. R., J. T. Snow, and J. Dessens. 1980. Intense atmospheric vortices associated with a 1000 MW fire. Bulletin of the American Meteorological Society 61:682-694.

Clements, W. E., J. A. Archuleta, and P. H. Gudiksen. 1989. Experimental design of the 1984 ASCOT field study. Journal of Applied Meteorology 28:405-413.

Dobosy, R. J., K. S. Rao, J. W. Przybylowicz, R. M. Eckman, and R. P. Hosker, Jr. 1989. Mass and momentum balance

in the Brush Creek drainage flow determined from single-profile data. Journal of Applied Meteorology 28:467-476.

Fast, J. D., and M. D. McCorcle. 1990. A two-dimensional numerical sensitivity study of the Great Plains low-level jet. Monthly Weather Review 118:151-163.

Gudiksen, P. H. 1983. ASCOT data from the 1980 field measurement program in the Anderson Creek Valley, California. ASCOT-83-1, Vol. 1, Lawrence Livermore National Laboratory, Livermore, California. 537 pp.

Haines, D. A. 1982. Horizontal roll vortices and crown fires. Journal of Applied Meteorology 21:751-763.

Haines, D. A., and M. C. Smith. 1987. Three types of horizontal vortices observed in wildland mass and crown fires. Journal of Climate and Applied Meteorology 26:1624-1637.

Haines, D. A., and M. C. Smith. 1992. Simulation of the collapse of bent-over vortex pairs observed in wildland fires. Forest Science 38:68-79.

Heilman, W. E., and J. D. Fast. 1991a. Two-dimensional numerical simulations of atmospheric conditions near lines of extreme surface heating. Proceedings of the 11th Conference on Fire and Forest Meteorology, (ed. P. L. Andrews and D. F. Potts), Society of American Foresters, 616 pp.

Heilman, W. E., and J. D. Fast. 1991b. Simulations of horizontal roll vortex development above lines of extreme surface heating. (Accepted), International Journal of Wildland Fire.

Heilman, W. E., and E. S. Takle. 1991. Numerical simulation of the nocturnal turbulence characteristics over Rattlesnake Mountain. Journal of Applied Meteorology 30:1106-1116.

Horst, T. W., and J. C. Doran. 1982. Simple nocturnal slope flow data from the Rattlesnake Mountain site. ASCOT-82-5, Pacific Northwest Laboratory, Richland, WA, 98 pp.

Horst, T. W., and J. C. Doran. 1986. Nocturnal drainage flow on simple slopes. Boundary- Layer Meteorology 34:263-286.

Leone, J. M., and R. L. Lee. 1989. Numerical simulation of drainage flow in Brush Creek, Colorado. Journal of Applied Meteorology 28:530-542.

Luti, F. M. 1980. Transient flow development due to a strong heat source in the atmosphere. Part 1: Uniform temperature source. Combustion Science and Technology 23:163-175.

Luti, F. M. 1981. Some characteristics of a two-dimensional starting mass fire with cross flow. Combustion Science and Technology 24:25-33.

Mahrer, Y., and R. A. Pielke. 1975. A numerical study of the air flow over mountains using the two-dimensional version of the University of Virginia mesoscale model. Journal of the Atmospheric Sciences 32:2144-2155.

Manins, P. C., and B. L. Sawford. 1979. Katabatic winds: A field case study. Quarterly Journal of the Royal Meteorological Society 105:1011-1025.

Martin, C. L., and R. A. Pielke. 1983. The adequacy of the hydrostatic assumption in sea breeze modeling over flat terrain. Journal of the Atmospheric Sciences 40:1472-1481.

McCorcle, M. D. 1988. Simulation of surface-moisture effects on the Great Plains low-level jet. Monthly Weather Review 116:1705-1720.

McNider, R. T., and R. A. Pielke. 1984. Numerical simulation of slope and mountain flows. Journal of Climate and Applied Meteorology 23:1441-1453.

Mellor, G. L., and T. Yamada. 1974. A hierarchy of turbulence closure models for planetary boundary layers. Journal of the Atmospheric Sciences 31:1791-1806.

Paulson, C. A. 1970. The mathematical representation of wind speed and temperature profiles in the unstable atmospheric surface layer. Journal of Applied Meteorology 9:857-861.

Rao, K. S., and H. F. Snodgrass. 1981. A nonstationary nocturnal drainage flow model. Boundary-Layer Meteorology 20:309-320.

Schaefer. V. J. 1957. The relationship of jet streams to forest fires. Journal of Forestry 55:419-425.

Smith, M. C., D. A. Haines, and W. A. Main. 1986. Some characteristics of longitudinal vortices produced by line-source heating in a low-speed wind tunnel. International Journal of Heat and Mass Transfer 29:59-68.

Smith, M. C., D. A. Haines, and W. A. Main. 1989. Growth of buoyancy-induced longitudinal vortex pairs in a laminar flow. International Journal of Heat and Mass Transfer 32:1879-1885.

Song, J. L., R. A. Pielke, M. Segal, R. W. Arritt, and R. C. Kessler. 1985. A method to determine nonhydrostatic effects within subdomains in a mesoscale model. Journal of the Atmospheric Sciences 42:2110-2120.

Stone, G. L., and D. E. Hoard. 1989. Low-frequency velocity and temperature fluctuations in katabatic valley flows. Journal of Applied Meteorology 28:477-488.

Whiteman, C. D., and S. Barr. 1986. Atmospheric mass transport by along-valley wind systems in a deep Colorado valley. Journal of Climate and Applied Meteorology 25:1205-1212.

Yamada, T. 1981. A numerical simulation of the nocturnal drainage flow. Journal of the Meteorological Society of Japan 59:108-122.

Yamada, T. 1983. Simulations of nocturnal drainage flows by a q^2-ℓ turbulence closure model. Journal of the Atmospheric Sciences 40:91-106.

Yamada, T., and S. Bunker. 1989. A numerical model study of nocturnal drainage flows with strong wind and temperature gradients. Journal of Applied Meteorology 28:545-554.